Available online at www.sciencedirect.com
SCIENCE DIRECT®
International Journal of Heat and Mass Transfer 47 (2004) 245–256
International Journal of HEAT and MASS TRANSFER
www.elsevier.com/locate/ijhmt

Influence of shaped injection holes on turbine blade leading edge film cooling

Youn J. Kim *, S.-M. Kim

School of Mechanical Engineering, SungKyunKwan University, 300 CheonCheon-dong, Suwon 400-746, South Korea

Received 13 May 2003; received in revised form 12 July 2003

Abstract

To improve the film cooling performance by shaped injection holes for the turbine blade leading edge region, we have investigated the flow characteristics of the turbine blade leading edge film cooling using five different cylindrical body models with various injection holes, which are a baseline cylindrical hole, two laidback (spanwise-diffused) holes, and two tear-drop shaped (spanwise- and streamwise-diffused) holes, respectively. Mainstream Reynolds number based on the cylinder diameter was 7.1×10^4 and the mainstream turbulence intensities were about 0.2%. The effect of injectant flow rates was studied for various blowing ratios of 0.7, 1.0, 1.3 and 1.7, respectively. The density ratio in the present study is nominally equal to one. Detailed temperature distributions of the cylindrical body surfaces are visualized by means of an infrared thermography (IRT). Results show that the conventional cylindrical holes have poor film cooling performance compared to the shaped holes. Particularly, it can be concluded that the laidback hole (Shape D) provides better film cooling performance than the other holes and the broader region of high effectiveness is formed with fairly uniform distribution.

1. Introduction

From a thermodynamic cycle analysis, it is found that the thermal efficiency of gas turbine engine can be improved by increasing turbine inlet temperature. However, a major problem associated in achieving the increased performance of gas turbine system is the availability of material that can withstand such high temperatures and combined stresses. Film cooling is one kind of cooling methods applied to gas turbine engine system. In a film cooled turbine blade, the coolant is injected into mainstream through discrete holes drilled along the blade surface. The coolant acts as a protective layer between the blade surface and the hot combustion gas. To develop the high efficient gas turbine engine, designers and researchers are trying to get greater cooling performance from less coolant. Studies on shaped injection holes and blowing ratios are aimed to these purposes.

Many experimental studies on shaped injection holes have been carried out. Goldstein et al. [1] were the first to pioneer the use of shaped injection hole for improving film cooling performance. They used a 10° spanwise-diffused hole and found that the shaped hole provides better film cooling characteristics than the cylindrical hole, because the reduced momentum of the jet attenuated coolant lift-off from the blade surface, and thus less penetration of the coolant into the mainstream. Sen et al. [2] and Schmidt et al. [3] examined the performance of 15° forward-diffused holes. They found that the forward-diffused holes show better performance than the cylindrical holes. Thole et al. [4] measured the flow fields of three different injection holes, which were a cylindrical hole, a laterally-diffused hole and a forward-laterally diffused hole, respectively. The results of their study showed that by diffusing the hole exit, both the penetration of the coolant into mainstream and the intense shear regions are significantly reduced relative to a cylindrical injection hole. Recently, Yu et al. [5] examined

* Corresponding author. Tel.: +82-31-290-7448; fax: +82-31-290-5849.
E-mail address: yjkim@skku.edu (Y.J. Kim).

0017-9310/$ - see front matter © 2003 Elsevier Ltd. All rights reserved.
doi:10.1016/j.ijheatmasstransfer.2003.07.008

Nomenclature

B	blowing ratio
D	diameter of cylindrical leading edge
DR	density ratio
d	diameter of cylindrical injection hole
I	momentum flux ratio
L	length of film hole passage
p	film hole pitch
Re_D	Reynolds number based on the diameter of cylindrical body model
T	temperature
U	velocity
x	streamwise direction along the blade surface from stagnation
X	mainstream direction
y	normal direction to the blade surface
Y	normal direction to the wall of the wind tunnel
z	lateral direction along the blade surface

Greek symbols

α	streamwise injection angle from stagnation
β	injection angle relative to spanwise direction
η	adiabatic film cooling effectiveness
$\bar{\eta}$	spanwise-averaged film cooling effectiveness
θ	angle from stagnation
ρ	density

Subscripts

aw	adiabatic wall
w	wall
c	coolant
∞	mainstream

Notations

Shape A	cylindrical hole with injection angle 30° relative to spanwise direction
Shape B	same with Shape A except the exit is opened by 10° in spanwise direction at $y = -0.87d$
Shape C	same with Shape B except the exit is opened by 10° in streamwise direction at $y = -0.87d$
Shape D	same with Shape A except the exit is opened by 10° in spanwise direction at $y = -1.15d$
Shape E	same with Shape D except the exit is opened by 10° in streamwise direction at $y = -1.15d$

that the combined forward- and lateral-diffused holes produce a significant increase in film performance compared to the cylindrical holes. However, most studies on the effects of shaped injection hole on the film-cooled turbine blade have been performed with flat plate not considering the case with curvature effects like a real turbine blade leading edge. Experimental studies on leading edge film cooling have been reported by Ou and Han [6], Mehendale and Han [7], Salcudean et al. [8], Ekkad et al. [9], Reiss and Bolcs [10], Ou and Rivir [11], Cruse et al. [12], and others. Especially, Cruse et al. [12] measured the surface temperature distributions of a blunt body with a circular leading edge and a flat afterbody using infrared technique.

In general, spatially-resolved temperature distributions along the blade surface are determined using infrared imaging in conjunction with thermocouples, digital image processing, and in situ calibration procedures. Infrared thermography (IRT) is commonly used to analyze convective heat transfer phenomena, as encountered in thermo-fluid problems. Some advantages of IRT, when compared to standard sensors, are that a truly two-dimensional temperature field can be obtained, since it allows for accurate measurements of surface temperature in the presence of high spatial temperature gradients after proper calibration. Furthermore, IRT is non-contact technique of temperature measurement, thus avoids the thermal conduction and the possibility of flow disturbances through the discretely placed thermocouple, which generally gives rise to errors in conventional measurements. It is additionally advantageous over liquid crystals (LCs), because it does not require the use of transient testing procedures, and LCs working range is generally quite limited.

In order to investigate the effects of shaped injection holes on the film cooling performance, we have investigated the leading edge film cooling, using five different cylindrical body models with various injection hole shapes, which are a baseline cylindrical hole, two laid-back (spanwise-diffused) holes, and two tear-drop shaped (spanwise- and streamwise-diffused) holes, respectively. Mainstream Reynolds number based on the cylinder diameter was 7.1×10^4. The turbulence intensities were about 0.2%. The effect of injectant flow rates was studied for different blowing ratios of 0.7, 1.0, 1.3 and 1.7, respectively. The temperature distributions on the cylindrical body surface are visualized by means of IRT.

2. Experimental apparatus and procedure

The overall experimental apparatus with the infrared camera oriented in a 45° scan angle set-up is shown in Fig. 1. The cross-sectional area of acrylic test section is

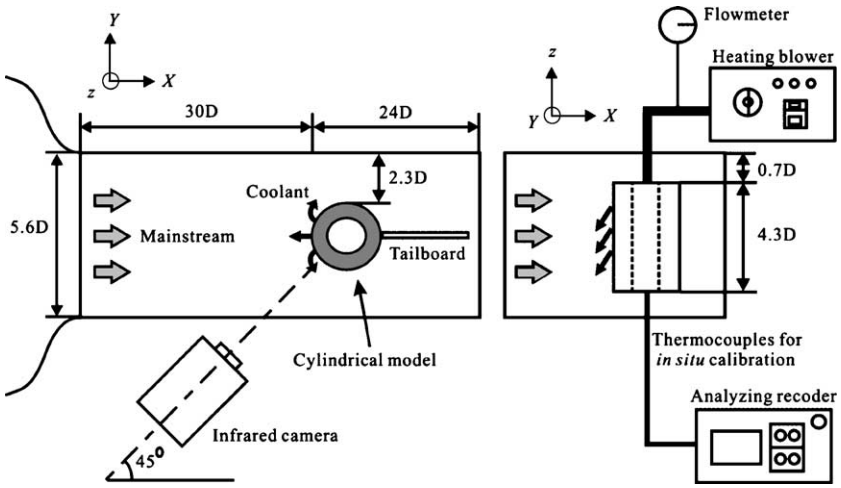

Fig. 1. Schematic diagram of experimental apparatus.

450 mm × 450 mm and its length is 4.3 m. Subsonic wind tunnel has contraction ratio of 7:1, and its maximum velocity and turbulence intensity are 45 m/s and 0.5% below, respectively. A honeycomb and four screens are placed in it for supplying uniform mainstream. The turbulence intensities are measured by 1-axis hot wire probe of IFA 300 (TSI). Auto traverse system was used to control the exact position of the probe. Fig. 2 shows the distribution of the turbulence intensities [%] over the cross-section at $1 \times D$ upstream of the cylindrical model except boundary layer region. It is seen that the turbulence intensities vary over the cross-section but show nearly uniform distribution about 0.2%. The spatial uniformity of average velocity is within ±1% except boundary layer region. To reduce the wake effect of the cylindrical model, a tailboard is installed at back of the model.

The cylindrical body models for simulating the turbine blade leading edge, scaled up by a factor of 4, are shown in Fig. 3. The model is made of polyacetal, which has low thermal conductivity of 0.15 W/m K, to reduce the axial and radial conduction along the model surface. The roughness of the model is less than 30 μm at the blade surface and less than 80 m at the film holes. The showerhead configuration consists of three staggered rows (nine holes in each row) with a leading edge diameter of $D = 80$ mm. Flow symmetry was established by tufts on the stagnation, and by checking the temperatures at corresponding locations on either side of the blade surface. Five different injection holes are introduced with referenced model of which has cylindrical hole with injection angle 30° relative to the spanwise direction (Shape A). The others are same with Shape A except the exit is opened by 10° in the spanwise direction at $y = -0.87d$ (Shape B), same with Shape B except the exit is opened by 10° in the streamwise direction at

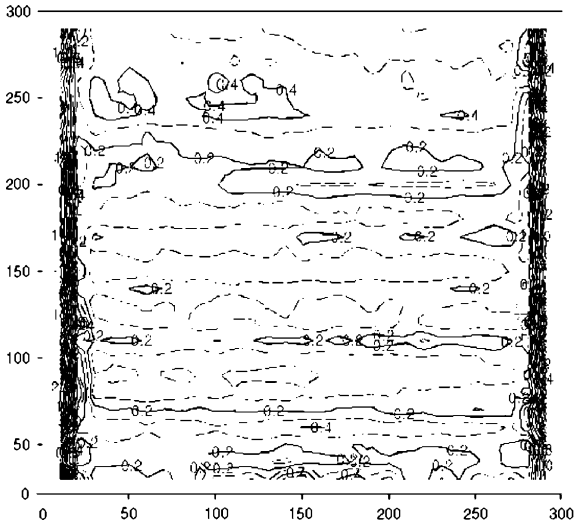

Fig. 2. Distribution of the turbulence intensities [%] over the cross-section at $1 \times D$ upstream of the cylindrical model except boundary layer region.

$y = -0.87d$ (Shape C), same with Shape A except the exit is opened by 10° in the spanwise direction at $y = -1.15d$ (Shape D), and same with Shape D except the exit is opened by 10° in the streamwise direction at $y = -1.15d$ (Shape E). They are arranged symmetrically with respect to the mainstream, at the streamwise direction 0°, ±23°, and a hole spacing of $p/d = 7.5$. Length-to-diameter ratio (L/d) is 8.0 (much larger than 4), thus, the entrance effect of the injectant is unimportant. The hole exit-to-entry area ratio of the Shapes A, B, C, D, and E is 2.0, 2.9, 3.5, 3.2 and 4.0, respectively. The letters α and β denote the streamwise injection angle from stagnation, and the injection angle relative to the

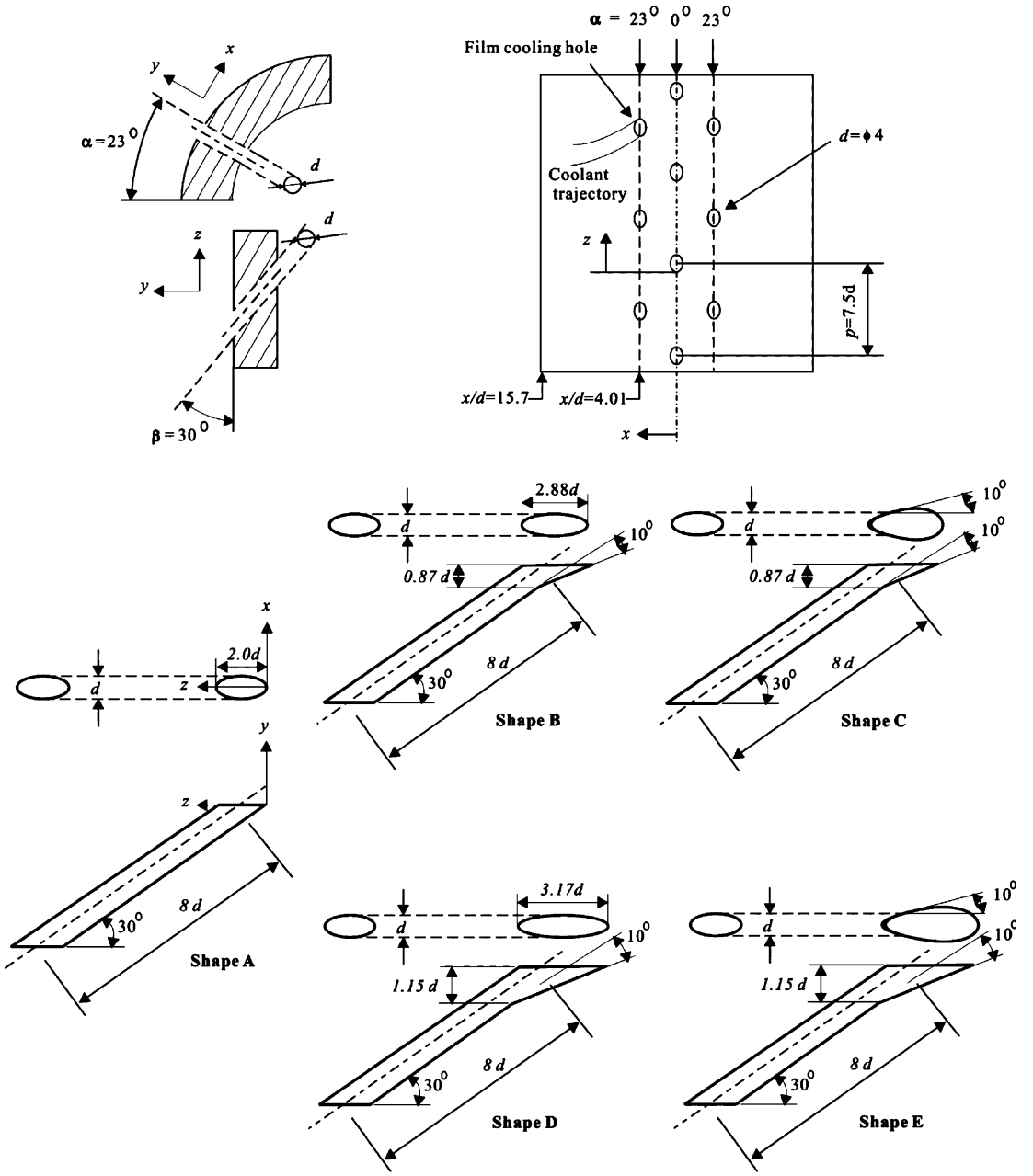

Fig. 3. Overview of hole geometries and coordinate systems.

spanwise direction, respectively. The coordinate system used is such that the x-axis is streamwise direction along the blade surface, the y-axis is normal direction to the blade surface, and the z-axis is lateral direction along the blade surface, respectively.

Blowing ratio (B) is one of dominant parameters in film cooling study. It is represented as the mass flux ratio between the mainstream and the coolant as follows:

$$B = \frac{\rho_c U_c}{\rho_\infty U_\infty} \tag{1}$$

In addition, momentum flux ratio (I) can be written as follows:

$$I = \frac{\rho_c U_c^2}{\rho_\infty U_\infty^2} \tag{2}$$

In the present study, the air was used for the coolant. Therefore, the blowing ratio is essentially the velocity ratio between the mainstream and the injected air (DR ≈ 1.0). The mainstream velocity is 14 m/s. Thus, Reynolds number (Re_D) based on D is about 7.1×10^4. Several experiments are conducted with various blowing ratios, 0.7, 1.0, 1.3 and 1.7, respectively (relevant moment flux ratio $I = 0.5$, 1.0, 1.7 and 2.9). The total injectant flow rates that are averaged for all injection holes were measured with an orifice type flowmeter. Injectant flow rates are adjusted until the desired blowing ratio, B, in Eq. (1) by controlling the flowmeter.

The experimental data are provided in the form of adiabatic film cooling effectiveness, which is defined as follows:

$$\eta = \frac{T_{aw} - T_\infty}{T_c - T_\infty} \tag{3}$$

where T_{aw} denotes the adiabatic wall temperature. With low thermal conductivity of test models, surface heat flux is minimal, creating a near adiabatic surface boundary condition. In hence, we may assume that the surface temperatures measured by IR-camera correspond to adiabatic wall temperatures. As the studies of Ou and Han [6], and Ekkad et al. [9], the injectant was heated above the mainstream temperature and the temperature difference between the injectant (about 30 °C) and the mainstream (about 10 °C) was maintained at 20 °C by automatic temperature controller in heating blower. A T-type thermocouple is located in the plenum and connected to automatic temperature controller to maintain the temperature difference.

The local film effectiveness measurements were used to find the spanwise-averaged film cooling effectiveness, which is given by:

$$\bar{\eta} = \sum(\eta \cdot \Delta z) \Big/ \sum \Delta z \tag{4}$$

To perform the in situ calibrations, analyzing recorder (DA100, YOKOGAWA) reads adiabatic wall temperature through T-type thermocouples at 20 points attached along the body surface. All thermocouple wires are extracted to the back of a cylindrical body model through plenum and connected to the analyzing recorder. The temperature distributions of the cylindrical body surface are measured by IRT (Varioscan 3011-ST, JENOPTIK), which operates at infrared wave lengths from 8 to 12 μm. The thermal resolution of this camera is ±0.03 K at 30 °C black-body radiator, and its frame repeat cycle is 0.8 s. The error on the measured temperature between the thermocouple and IRT depends strongly on the emissivity of the model surface; however, an error in the evaluation of the emissivity coefficient leads, in most cases, to a smaller error of the measured temperature [13]. The model surface was covered with a thin layer of a black paint that exhibits a high emissivity required by infrared camera measurements. All measurements in this study are obtained when each of the temperatures from the 20 thermocouples along the body surface vary by less than 0.1 °C. A linear calibration curve was applied to the camera readings for wall temperatures of $5 \leqslant T_w \leqslant 35$ °C, and had a standard deviation of 0.2 °C. In situ calibration results of the infrared system are also given by Meinders et al. [14] and by Hedlund et al. [15].

Captured infrared images of cylindrical body surface are converted to ASCII format (temperature at each pixel location) using the Visual C++, and then determines the values of local adiabatic effectiveness. This program is also used to perform coordinate transformations to correct for distorted recorded images because of camera perspective or camera lens orientation is not normal to the curved surface.

3. Uncertainty estimates

Uncertainty estimates are performed by based on 20 to 1 odds (95% confidence level), and obtained by the procedure described by Kline and McClintock [16] and Moffat [17]. The Reynolds number uncertainty is ±120. Uncertainty in measuring the flow rate of the air supply system was about 4%. Uncertainty in a thermocouple measurement is believed to be 0.2 °C. The captured infrared image covers 110×170 pixel area. Spatial and temperature resolution achieved with infrared imaging are 0.29 mm × 0.33 mm per pixel (averaged in the streamwise direction) and 0.2 °C, respectively. The local adiabatic effectiveness uncertainty is then ±0.013 at $\eta = 0.2$, and ±0.012 at $\eta = 0.5$.

4. Results and discussion

Figs. 4–8 show the detailed film cooling effectiveness distributions at the leading edge surface measured by IR-camera for all five hole configurations with $B = 0.74$, 1.0, 1.3 and 1.7. The mainstream direction is toward the top, and the injectant supply to the plenum comes from the right. Although injectant flow rates in each hole vary with the flow resistance distribution along the spanwise direction, temperature contour of the surface showed relatively good periodicity along the spanwise direction, and confirmed flow symmetry in the stagnation. Figs. 9–13 show the spanwise-averaged film cooling effectiveness along the streamwise direction at 80 picked points with a spacing of $x/d = 0.16$, which are selected from 170 data points in the streamwise direction for clear distinction of graphs. These data are the averaged values of local adiabatic effectiveness at 110 pixels in the spanwise direction. The film cooling effectiveness has a peak value

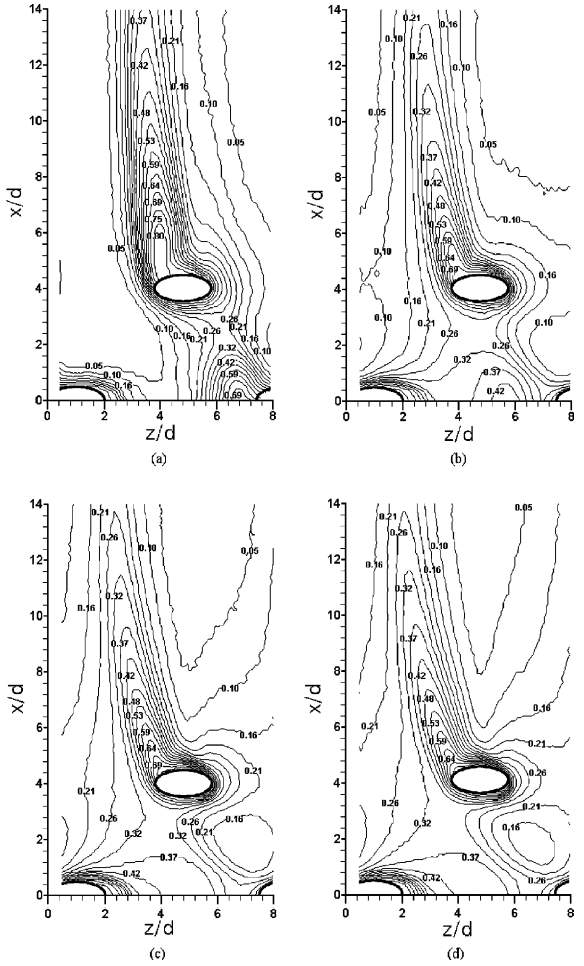

Fig. 4. Film cooling effectiveness distributions at the leading edge surface for Shape A. (a) $B = 0.7$, (b) $B = 1.0$, (c) $B = 1.3$, (d) $B = 1.7$.

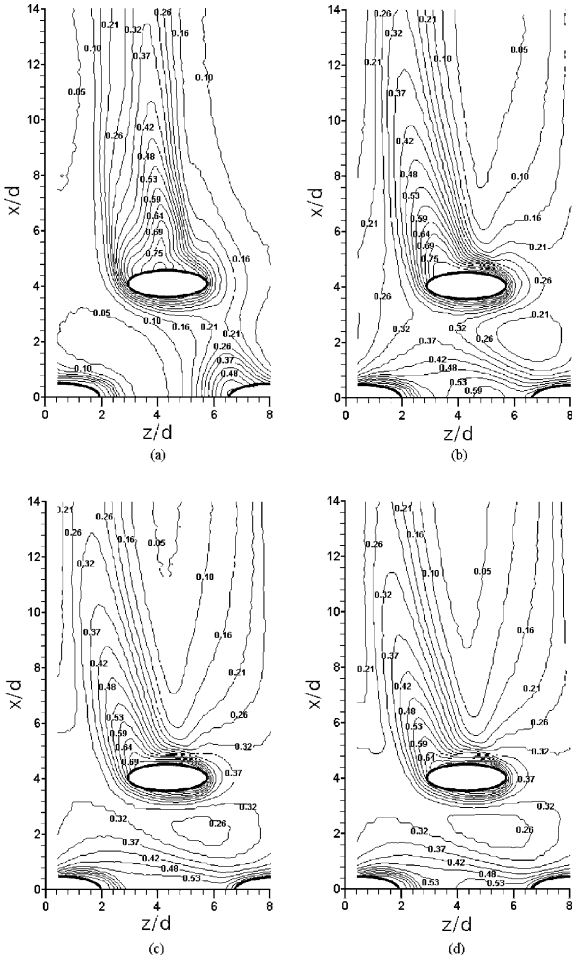

Fig. 5. Film cooling effectiveness distributions at the leading edge surface for Shape B. (a) $B = 0.7$, (b) $B = 1.0$, (c) $B = 1.3$, (d) $B = 1.7$.

at the vicinity of the injection holes and decreases with x/d due to increase in the mixing between the mainstream and the injectant.

As shown in the film cooling effectiveness distributions at the leading edge surface (refer to Figs. 4–8), for lower blowing ratio ($B = 0.7$), the trajectory of the first-row merges into the exit of the second-row, and the trajectory of the second-row is nearly aligned with mainstream direction. However, as the blowing ratio increases, the trajectory of the second-row deviates from the hole centerline. Also, the pressure difference across the first-row hole is smaller than that across the second-row hole due to the pressure distribution around the cylinder surface. Particularly, with lower blowing ratio, it can clearly be seen that the mass flow rate of the injectant through the first-row hole is much less than that through the second-row hole for all injection hole models. This was also observed by Reiss and Bölcs [10], and Lin and Shih [18]. In addition, at lower blowing ratio, the low effectiveness region between the first-row holes exists near the stagnation region ($3 < z/d < 5$), and is reduced as the blowing ratio increases.

4.1. Cylindrical injection holes

As shown in Fig. 4, the injectant through the first-row hole can be seen to flow mainly in the spanwise direction due to the strong lateral momentum of the jet. Some injectant through the first-row hole can also be seen to flow in the streamwise direction because the boundary layer is very thin and the mainstream velocity is very low around the stagnation region [11,18]. As the blowing ratio increases, the adiabatic effectiveness near the first-row hole shows relatively lower value between $6 < z/d < 7$ (refer to Fig. 4(c) and (d)), namely, for typical cylindrical holes (Shape A), the injectant through

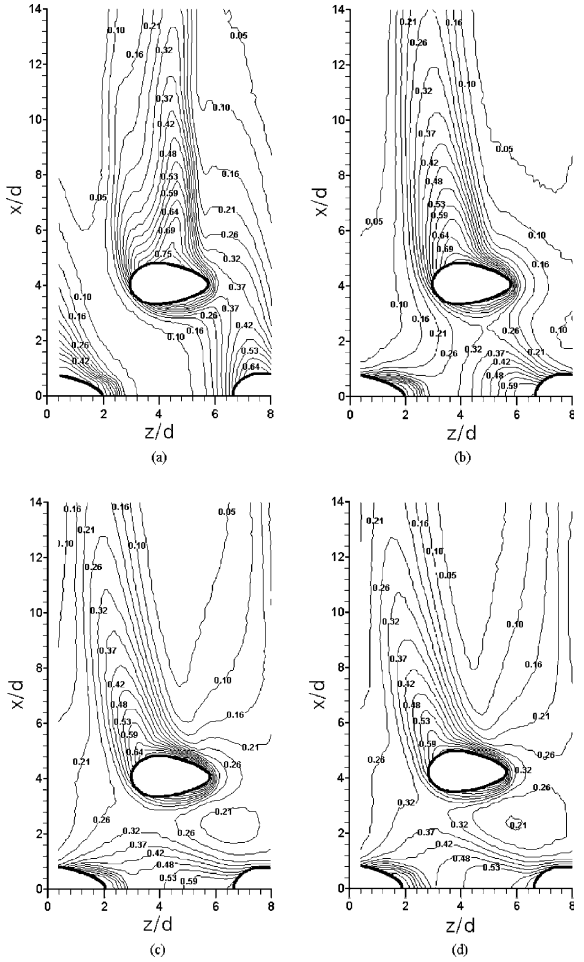

Fig. 6. Film cooling effectiveness distributions at the leading edge surface for Shape C. (a) $B = 0.7$, (b) $B = 1.0$, (c) $B = 1.3$, (d) $B = 1.7$.

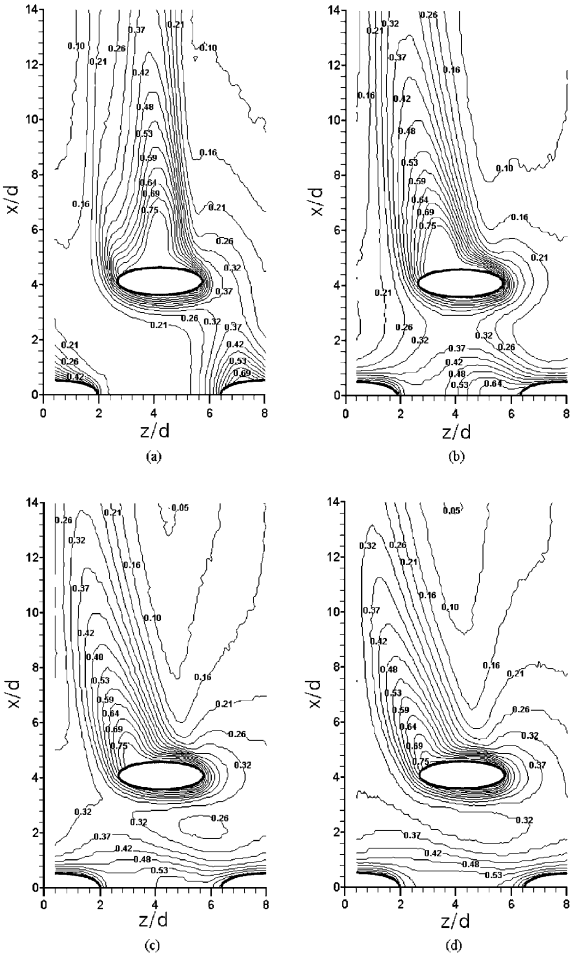

Fig. 7. Film cooling effectiveness distributions at the leading edge surface for Shape D. (a) $B = 0.7$, (b) $B = 1.0$, (c) $B = 1.3$, (d) $B = 1.7$.

the first-row hole detaches from the surface due to the strong exit momentum.

The injectant through the second-row hole interacts strongly with the mainstream due to the higher mainstream velocity at this location. This interaction causes the mainstream to be entrained by the injectant and drawn to the surface. Therefore, it is noted that the injectant through the second-row hole is less effective than the first-row hole. As the blowing ratio increases, it can be seen that the trajectory of the second-row gets smaller and more deviates from the hole centerline. In addition, the film cooling effectiveness decreases in the vicinity of the second-row hole ($x/d = 5$). This is because the injectant having strong exit momentum lifts off and separates from the surface. As shown in Fig. 9, the effectiveness increases rapidly, as the blowing ratio increases (until $B = 1.3$). However, the effectiveness for $B = 1.3$ is nearly same with that for $B = 1.7$. This may suggest the injectant lift-off from the surface by increasing the blowing ratio.

4.2. Shaped injection holes

4.2.1. At the first-row holes

Film-cooling performance can be significantly improved by controlling the injection hole shape. Walters and Leylek [19] observed that the low-momentum region along the downstream side (trailing edge) of the jet stream and a corresponding high momentum or jetting region along the upstream side (leading edge) within the film cooling hole. To increase this low-momentum region near the hole exit, the four diffused injection holes were used. The laidback holes, Shape B (same with Shape A except the exit is opened by 10° in the spanwise direction at $y = -0.87d$) and Shape D (same with Shape A except the exit is opened by 10° in the spanwise

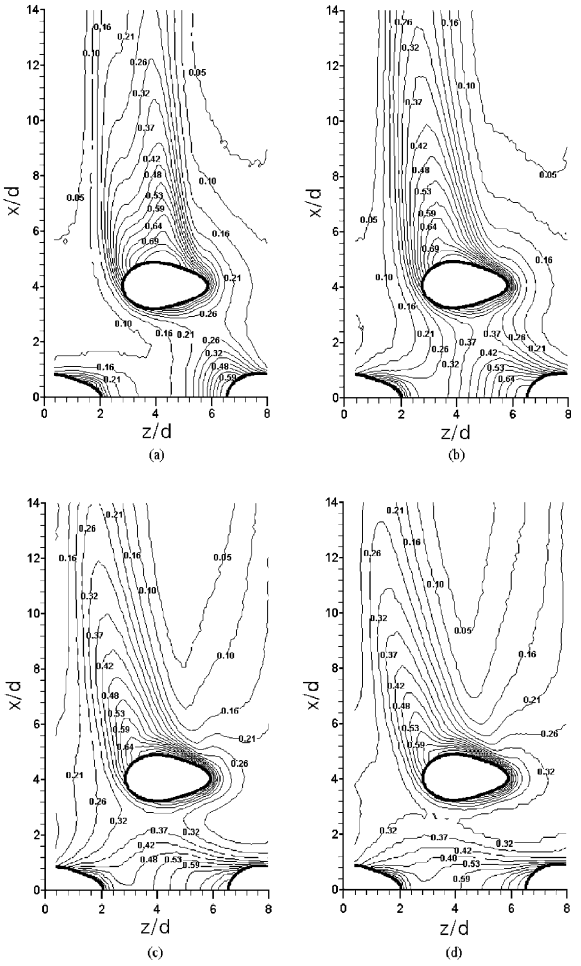

Fig. 8. Film cooling effectiveness distributions at the leading edge surface for Shape E. (a) $B = 0.7$, (b) $B = 1.0$, (c) $B = 1.3$, (d) $B = 1.7$.

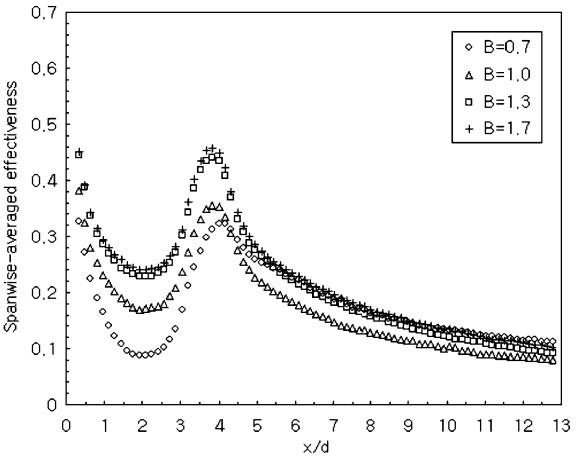

Fig. 9. Spanwise-averaged film cooling effectiveness for Shape A.

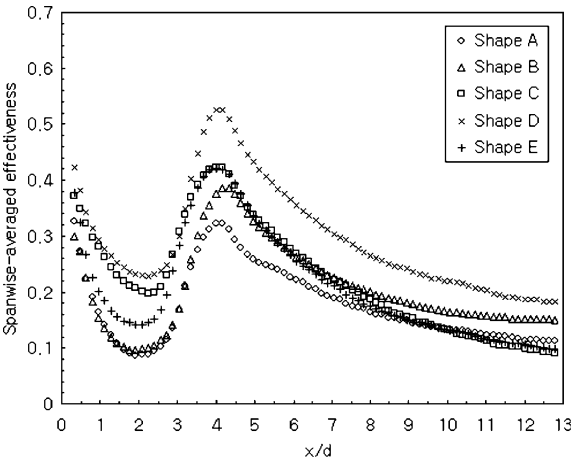

Fig. 10. Spanwise-averaged film cooling effectiveness for $B = 0.7$.

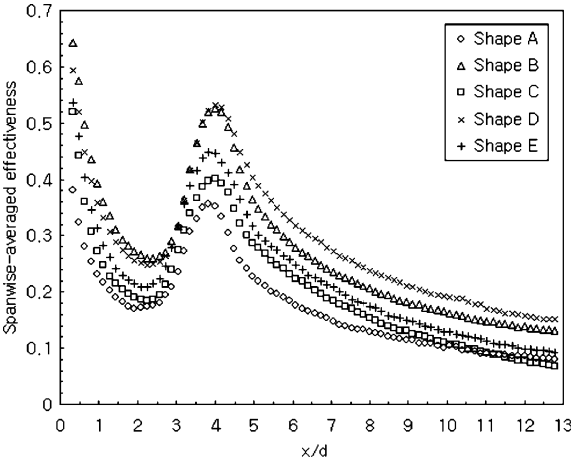

Fig. 11. Spanwise-averaged film cooling effectiveness for $B = 1.0$.

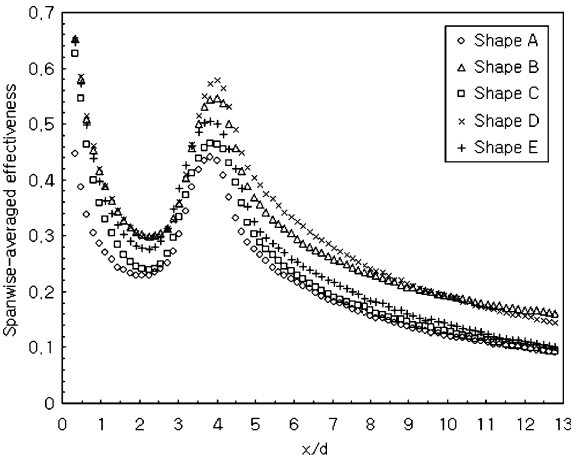

Fig. 12. Spanwise-averaged film cooling effectiveness for $B = 1.3$.

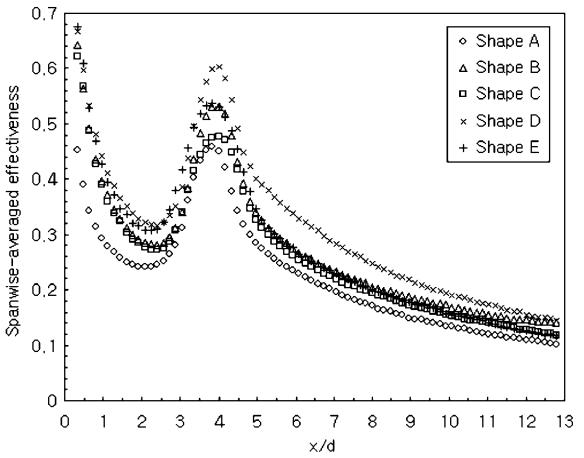

Fig. 13. Spanwise-averaged film cooling effectiveness for $B = 1.7$.

direction at $y = -1.15d$), are designed to increase the lateral momentum of the injectant by spanwise diffusion of the hole exit compared to Shape A. The tear-drop shaped holes, Shape C (same with Shape B the exit is opened by 10° in the streamwise direction at $y = -0.87d$) and Shape E (same with Shape D except the exit is opened by 10° in the streamwise direction at $y = -1.15d$), are intended to increase low-pressure region near the hole exits by more expanding the hole exits compared to Shapes B and D.

Aforementioned, for $B = 0.7$, it is observed that the injectant through the first-row having low exit momentum provides weak lateral spreading, thus, the low effectiveness region between the first-row holes exists near the stagnation region (see $3 < z/d < 5$ in Figs. 5–8). For $B = 1.0$, the injectant through Shapes B and D having strong lateral momentum by spanwise diffusion of the hole exit shows relatively uniform distributions of film cooling effectiveness at the stagnation region. However, the injectant through Shapes C and E having weak lateral momentum provides poor lateral spreading and merges with the injectant through the second-row. For example, near $z/d = 3.0$, Shapes B and D show relatively higher film effectiveness than Shapes C and E, while, near $z/d = 6.0$ at $x/d = 2.0$, Shapes B and D show lower film cooling effectiveness than Shapes C and E. In addition, as shown in Fig. 11, the spanwise-averaged effectiveness of Shapes B and D is approximately 42% and 19% higher than that of Shapes C and E at $x/d = 2.08$, respectively.

For $B = 1.3$, all shaped models provide comparatively uniform distributions of film cooling effectiveness at the stagnation region. Particularly, low effectiveness regions (near $z/d = 3.0$) of Shapes C and E are reduced, as compared with the case of $B = 1.0$. For Shapes B and D, it is seen that the injectant through hole exit located at near $z/d = 8$ covers the vicinity of adjacent hole at near $z/d = 1$ due to strong lateral momentum, as compared to Shapes C and E. Also, at downstream of the first-row ($x/d = 2.0$), Shapes B and D shows higher film cooling effectiveness than Shapes C and E. Especially, it is noted that Shape C near $0.4 < z/d < 1$ and $5 < z/d < 8$ shows poor performance due to weak lateral momentum, thus, Shape C at downstream of the first-row has lower spanwise-averaged effectiveness than other shaped holes (refer to Fig. 12). For $B = 1.7$, as shown in Fig. 13, all shaped models show better cooling performance than cylindrical hole. Particularly, Shapes D and E provide higher film cooling effectiveness distributions than Shapes B and C. In addition, at $x/d = 2.08$, the effectiveness of Shape B is approximately 6% lower than that for the case of $B = 1.3$. This may suggest that Shape B is more influenced by increasing the blowing ratio, as compared with other shaped holes, due to the injectant lift-off.

4.2.2. At the second-row holes

The laidback holes, Shapes B and D, show much higher film effectiveness, broader and more inclined trajectory to the hole centerline than cylindrical holes at the second-row (see Figs. 5 and 7). For example, for $B = 1.3$ at $x/d = 5.92$, the spanwise-averaged effectiveness of Shapes B and D is 37% and 51% higher than that of Shape A, respectively. This is because of increased lateral momentum of the injectant by spanwise diffusion of the hole exit which causes less penetration into the mainstream and the injectant to be more spread out to the spanwise direction. For all blowing ratios, Shape D shows highest film cooling effectiveness among the five hole shapes studied. Particularly, for higher blowing ratios ($B = 1.7$), Shape D provides better cooling performance and its effect remains further downstream. As shown in Fig. 13, for $B = 1.7$, Shapes B, C and E at the second-row show film cooling effectiveness values on approximately the same level. However, Shape D provides much higher film cooling effectiveness. For instance, its spanwise-averaged effectiveness is about 43%, 23%, 30%, and 24% higher than that of Shapes A, B, C and E at $x/d = 5.92$, respectively. This may be due to less significant injectant lift-off from the surface for Shape D.

On the other hand, it is seen from Figs. 10–13 that the tear-drop shaped holes, Shapes C and E, represent relatively low effectiveness than Shapes B and D for $B = 1.0$ and 1.3 except for $B = 0.7$. This is because of the insufficient lateral momentum of the injectant by additional streamwise expansion. As mentioned before, the expanded cross-sectional area at the exit of injection holes decreases the exit momentum of the injectant, therefore, reduces the penetration of the jet into the mainstream, as compared with the cylindrical holes.

In addition, enhanced lateral diffusion of the injectant through the laidback (spanwise-diffused) holes having strong lateral momentum causes an increased film cooling performance, as compared with the teardrop shaped (spanwise- and streamwise-diflused) holes, particularly at high blowing ratios. It can also be seen that Shape D having larger expanded area than Shape B provides better film cooling performance than other holes and the broader region of high effectiveness is formed with fairly uniform distribution. However, for a larger expanded hole, flow separation in the diffuse section of the film hole could occur, thus, the adequate design of hole shape must be made.

4.3. Comparison with other results

The measured film cooling effectiveness was compared with the results reported by Ou and Rivir [11], and Cruse et al. [12], considering the differences in the leading-edge model and experimental conditions. The film cooling effectiveness of current measurement (0.29 mm×0.33 mm per pixel) shows high spatial resolution compared to the studies of Ou and Rivir [11] (0.6 mm×0.6 mm per pixel), and Cruse et al. [12] (3 mm×3 mm per pixel).

As shown in Fig. 14(b), the film effectiveness distribution of Ou and Rivir [11], measured by using LC image technique ($\alpha = 0°$ and $\pm 21.5°$, $\beta = 20°$, $p/d = 7.86$, $Re_D = 6.0 \times 10^4$, $B = 2.5$, and DR = 1.0), shows more asymmetric trajectory of the injectant than that of current measurement. The difference with our data is mainly result of the difference in injection angle relative to the spanwise direction ($\beta = 20°$). Therefore, the injectant of Ou and Rivir [11] causes less penetration into the mainstream and close attachment to the blade surface, thus, the spanwise-averaged effectiveness is higher (see Fig. 15). Aforementioned, in current measurement ($\beta = 30°$), the spanwise-averaged effectiveness for $B = 1.3$ is almost same with that for $B = 1.7$ due to the injectant lift-off from the surface (refer to Fig. 9). However, in the work of Ou and Rivir [11], injectant lift-

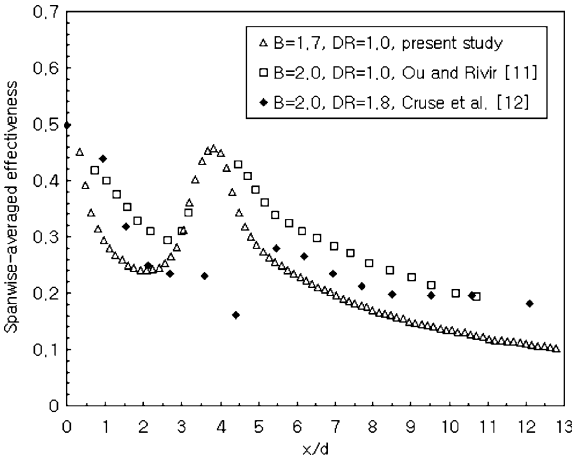

Fig. 15. Comparison of spanwise-averaged effectiveness to published data.

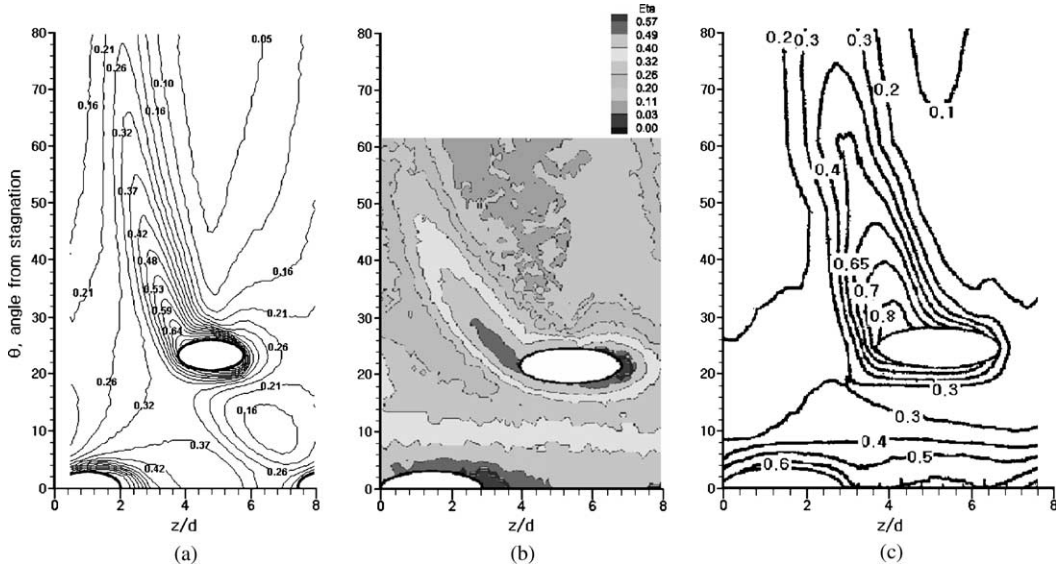

Fig. 14. Film cooling effectiveness distributions from: (a) present study ($B = 1.7$), (b) Ou and Rivir [11], and (c) Cruse et al. [12].

off occurs above $B = 2.0$ due to reduced injection angle relative to the spanwise direction.

Fig. 14(c) shows the film effectiveness distribution of Cruse et al. [12], measured by using infrared technique ($\alpha = 0°$ and $\pm 25°$, $\beta = 20°$, $p/d = 7.6$, $Re_D = 6.5 \times 10^4$, $B = 2.0$, and DR = 1.8). Although studies of Ou and Rivir [11] and Cruse et al. [12] are similar in hole inclined angles and blowing ratio, the injectants of the second-row show fairly different trajectory and the order of magnitude of the numbers is different. This is because the momentum flux ratio ($I = 4$) of Ou and Rivir [11] is higher than that ($I = 2.2$) of Cruse et al. [12], thus, the injectant trajectory more deviates to the hole centerline due to increased lateral momentum of the injectant, and the spanwise-averaged effectiveness of Ou and Rivir [11] is higher than that of Cruse et al. [12].

5. Concluding remarks

To improve the film cooling performance by shaped injection holes for the turbine blade leading edge region, we have studied the film cooling characteristics using cylindrical body model with five different injection holes. It is noted that the blowing ratio has a very strong effect on film cooling effectiveness and injectant trajectory is sensitive to the blowing ratio. For a typical cylindrical hole (Shape A), it is observed that the injectant lifts off and separates from the surface as the blowing ratio increases. It is also seen that Shape B is more influenced by increasing the blowing ratio, as compared with other shaped holes.

The film-cooling performance can be significantly improved by controlling the injection hole shape. The laidback holes (Shapes B and D) show much higher film cooling effectiveness, broader and more inclined trajectory to the hole centerline than cylindrical holes at second-row because of strong lateral momentum of the injectant by spanwise diffusion of the hole exit. However, the tear-drop shaped holes (Shapes C and E) present relatively low effectiveness than Shapes B and D because of the insufficient lateral momentum of the injectant by additional streamwise expansion. For all blowing ratios, Shape D shows highest film cooling effectiveness among the five hole shapes studied. Particularly, for higher blowing ratios ($B = 1.7$), Shape D provides better cooling performance and its effect remains further downstream.

Acknowledgements

The authors are grateful for the financial support provided by the Korea Science and Engineering Foundation through the Center for Advanced Plasma Surface Technology (CAPST) at the SungKyunKwan University. Financial aid also from the Korea Ministry of Education through the Brain Korea 21 project is gratefully acknowledged.

References

[1] R.J. Goldstein, E.R.G. Eckert, R. Burggraf, Effects of hole geometry and density on three dimensional film cooling, Int. J. Heat Mass Transfer 17 (1974) 595–606.
[2] B. Sen, D.L. Schmidt, D.G. Bogard, Film cooling with compound angle holes: heat transfer, ASME J. Turbomach. 118 (1996) 800–806.
[3] D.L. Schmidt, B. Sen, D.G. Bogard, Film cooling with compound angle holes: adiabatic effectiveness, ASME J. Turbomach. 118 (1996) 807–813.
[4] K. Thole, M. Gritsch, A. Schulz, S. Wittig, Flowfield measurements for film-cooling holes with expanded exits, ASME J. Turbomach. 120 (1998) 327–336.
[5] Y. Yu, C.H. Yen, T.I.P. Shih, M.K. Chyu, S. Gogineni, Film cooling effectiveness and heat transfer coefficient distributions around diffusion shaped holes, ASME J. Heat Transfer 124 (2002) 820–827.
[6] S. Ou, J.C. Han, Leading edge film cooling heat transfer through one row of inclined film slots and holes including mainstream turbulence effects, ASME J. Heat Transfer 116 (1994) 561–569.
[7] A.B. Mehendale, J.C. Han, Reynolds number effect on leading edge film effectiveness and heat transfer coefficient, Int. J. Heat Mass Transfer 36 (1993) 3723–3730.
[8] M. Salcudean, I. Gartshore, K. Zhang, I. McLean, An experimental study of film cooling effectiveness near the leading edge of a turbine blade, ASME J. Turbomach. 116 (1994) 71–79.
[9] S.V Ekkad, J.C. Han, H. Du, Detailed film cooling measurements on a cylindrical leading edge model: effect of free-stream turbulence and coolant density, ASME J. Turbomach. 120 (1998) 799–807.
[10] H. Reiss, A. Bölcs, Experimental study of showerhead cooling on a cylinder comparing several configurations using cylindrical and shaped holes, ASME J. Turbomach. 122 (2000) 161–169.
[11] S. Ou, R.B. Rivir, Egde film cooling heat transfer with high free stream turbulence using a transient liquid crystal image method, Int. J. Heat Fluid Flow 22 (2001) 614–623.
[12] M.W. Cruse, U.M. Yuki, D.G. Bogard, Investigation of various parametric influences on leading edge film cooling, ASME paper 97-GT-296, 1997.
[13] G.M. Carlomagno, L. de Luca, Infrared thermography in heat transfer, in: W.J. Yang (Ed.), Handbook of Flow Visualization, Hemisphere, London, 1989, pp. 531–553.
[14] E.R. Meinders, G.M.P. Kempen, L.J. Vliet, T.H. Meer, Measurement and application of an infrared image restoration filter to improve the accuracy of surface temperature measurements of cubes, Experim. Fluid 26 (1999) 86–96.
[15] C.R. Hedlund, P.M. Ligrani, B. Glezer, H.K. Moon, Heat transfer in a swirl chamber at different temperature ratios

and Reynolds numbers, Int. J. Heat Mass Transfer 42 (1999) 4081–4091.
[16] S.J. Kline, F.A. McClintock, Describing uncertainties in single sample experiments, Mech. Eng. 75 (1) (1953) 3–8.
[17] R.J. Moffat, Describing the uncertainties in experimental results, Experim. Therm. Fluid Sci. 1 (1) (1988) 3–17.
[18] Y.L. Lin, T.I.P. Shih, Film cooling of a cylindrical leading edge with injection through rows of compound angle holes, ASME J. Heat Transfer 123 (2001) 645–653.
[19] D.K. Walters, J.H. Leylek, A detailed analysis of film-cooling physics. Part I—Streamwise injection with cylindrical holes, ASME J. Turbomach. 122 (2000) 102–112.